ARTICLE

Luminescent $CaTiO_3$:Yb,Er Nanofibers Co-conjugated with Rose Bengal and Gold Nanorods for Potential Synergistic Photodynamic/Photothermal Therapy

Received 00th January 20xx,
Accepted 00th January 20xx

DOI: 10.1039/x0xx00000x

www.rsc.org/

Yike Fu[a†], Heng Liu[a†], Zhaohui Ren[a], Xiang Li[a]*, Jie Huang[b], Serena Best[c], Gaorong Han[a]*

Photodynamic therapy (PDT) and photothermal therapy (PTT) have been explored widely for application in cancer treatment. In this work, we describe the synthesis of $CaTiO_3$:Yb,Er (CTO) nanofibers co-conjugated with Rose Bengal (RB) and gold nanorods (AuNRs), which offer the potential for combined upconversion photoluminescence (UCPL) and enhanced, synergistic PDT and PTT. Based on this delivery platform, RB and AuNRs served as the PDT and PTT agents, respectively. RB and AuNRs have strong and well-matched absorption with the green and red emissions of UCPL CTO nanofibers respectively, hence a single 980 nm continuous wave laser with deep tissue penetration can be employed to allow PDT and PTT to occur simultaneously. The nanocomposite can effectively convert the near-infrared (NIR) radiation from the laser into a combination targeted hyperthermia and generation of reactive oxygen species (ROS). In comparison with PDT alone, the combined PDT/PTT treatment showed significantly enhanced suppression of the viability of Hep G2 cells *in vitro*, demonstrating its potential for use in oncology.

1 Introduction

Mortality due to cancer is increasing year on year and in 2012, an estimated 14.1 million new cancer cases and 8.2 million cancer deaths occurred worldwide.[1] Conventional cancer treatments including chemotherapy and radiotherapy are associated with a number of limitations, such as toxic side effects and the tendency towards multidrug resistance (MDR).[2, 3] These treatments may also fail to eradicate the tumor as expected. In recent years, drug-free phototherapy including photothermal therapy (PTT) and photodynamic therapy (PDT) have attracted increasing attention due to their unique advantages, which include low toxicity, low level side effects, possibilities for remote control, potential for minimally invasive intervention and avoidance of chemo-resistance.[4-9] Near-infrared (NIR) illumination has been recognized to be ideal for phototherapy applications due to its deep tissue penetration. Previous reports describe a penetration depth of at least 10 cm through breast tissue, and 4 cm of skull/brain tissue or deep muscle using NIR laser sources.[10] In general, PTT uses photo–absorbing agents to convert the electromagnetic energy of NIR light into localised heat and thereby destroy tumors via hyperthermia. For PDT, visible light converted by up-conversion nanomaterials under NIR light can activate photosensitizers (PSs) to generate cytotoxic reactive oxygen species (ROS), such as singlet oxygen ($^1O_2$), superoxide anions, and hydrogen peroxide, and thus reduce significantly the viability of tumor cells.[11-13] However, issues such as low potency, the requirement for excessive laser power density, high oxygen dependence and long-term skin photosensitization have significantly hindered the clinical translation of both techniques.[14]

Recent investigations have endeavored to develop synergistic therapeutic approaches in which PTT and PDT are combined effectively and simultaneously. Compared with individual treatment protocols, synergistic combined use of PTT and PDT can reduce the drawbacks of each method when used alone. Various types of nanocarriers, including gold nanomaterials[8, 15], graphene[16], and conjugated polymers[17], have been tested for combined PDT and PTT. For example, PDT/PTT dual-mode therapeutic agents based on Chlorin e6 (Ce6) modified poly(dopamine) nanospheres with high ROS generation and photothermal conversion efficiency was reported to offer significantly improved therapeutic effects as compared with PDT and PTT alone.[11]

[a] State Key Laboratory of Silicon Materials, School of Materials Science and Engineering, Zhejiang University, Hangzhou, Zhejiang 310027, P. R. China.
[b] Department of Mechanical Engineering, University College London, London WC1E 7JE, UK.
[c] Department of Materials Science and Metallurgy, University of Cambridge, Cambridge CB3 0FS, UK.
[d] * E-mail: xiang.li@zju.edu.cn; hgr@zju.edu.cn
† Authors contributed equally to this work.

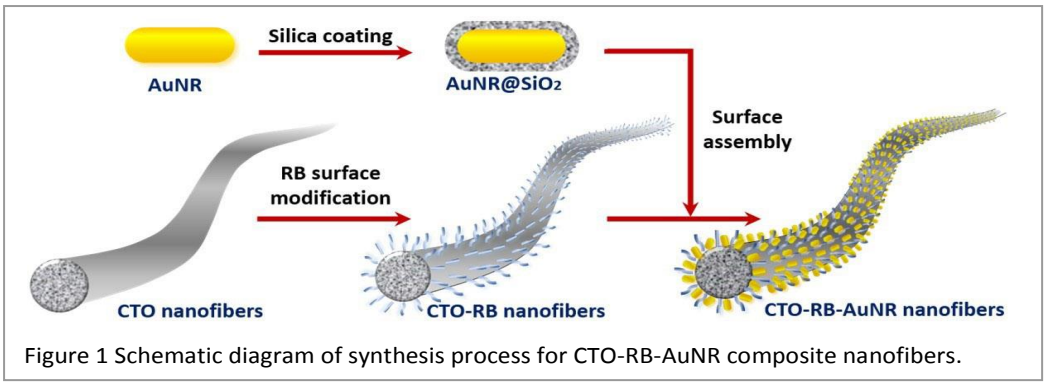

Figure 1 Schematic diagram of synthesis process for CTO-RB-AuNR composite nanofibers.

To date, a variety of ultraviolet light or visible light responsive photosensitizers including Ce6 (660 nm) and Photofrin (630 nm) have been investigated.[18-20] In such regions of the electromagnetic spectrum, light penetration is hindered due to endogenous chromophores and light scattering.[21] Therefore, two or more separate spectra with different wavelengths would normally be utilized for sequential excitation of each therapeutic step because of the absorption mismatch between photosensitizers and photothermal agents. However, sequential irradiation complicates and prolongs the treatment process owing to difficulties in focusing the two laser beams at the same position. Hence, constructing a novel therapeutic platform which can be triggered by a single wavelength laser for simultaneous PDT and PTT has become a hot topic in cancer therapy.

Another problem associated with PDT and PTT monotherapies is the target specificity of particulate PS/photothermal agents or their carriers. The low efficiency of delivery of PS/photothermal agents to tumour sites limits effectiveness of the treatment. Implantable therapeutic platforms, such as hydrogels and polymeric films etc., have been considered as an ideal substitutes for delivering PS/photothermal agents, which can achieve a much higher concentration of agents at the cancerous site and low systemic agent levels simultaneously.[22, 23] The design of phototherapeutic platforms based on the concept of localized drug delivery can maximize the effectiveness of PDT/PTT while minimizing the side effects of conventional therapy.

Calcium titanate ($CaTiO_3$) is a ceramic with excellent biocompatibility for medical implants.[24-26] The construction of rare earth doped $CaTiO_3$ nanofibers in our previous research also demonstrated the potential of capitalizing on the UCPL behaviour of $CaTiO_3$ for drug delivery applications.[27, 28] The rare earth ions doped, generally occupy the Ca site and the asymmetric perovskite structure of $CaTiO_3$ can effectively prohibit the possible diffusion of rare earth elements, which ensures the photoluminescent properties and avoids potential toxicity. In an advancement our previous work, an implantable nanocomposite based on these $CaTiO_3$ nanofibers has now been developed that allow us to combine PDT and PTT synergistically, in a way that offers the potential for a drug-free treatment regime. Rose Bengal (RB), a typical photodynamic therapeutic agent in the visible region, was attached to the surface of electrospun nanofibers comprising up-conversion photoluminescence (UCPL) $CaTiO_3$:Yb,Er (CTO) (Figure 1). In addition, silica-coated gold nanorods (AuNR@SiO_2) were prepared and anchored onto the nanofibers to serve as the photothermal agent. Using a single, 980 nm continuous wave laser, the red and green emissions from CTO nanofibers were absorbed by RB and AuNRs, generating a combination of heat and reactive oxygen species, respectively. The photothermal and photodynamic properties were analyzed systematically and an *in vitro* Hep G2 liver cancer cell model was utilized to evaluate the effects of the combined therapy compared with monotherapy. This work aims to find an effective approach for synergistic cancer therapy with superior efficacy.

2 Results and discussion

2.1 Characteristics of CTO nanofibers

Electrospun CTO nanofibers were prepared using a sol-gel precursor and were calcined at 700 °C. It has been shown previously that this provided fibers with the optimum combination of surface roughness and crystallinity (without the formation of a second phase) in the case of subsequent attachment of active drug molecules.[27] Representative

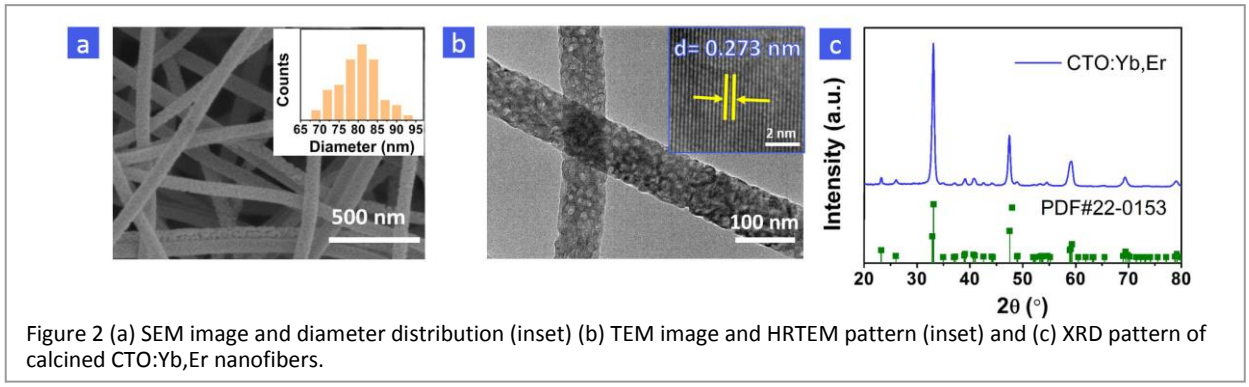

Figure 2 (a) SEM image and diameter distribution (inset) (b) TEM image and HRTEM pattern (inset) and (c) XRD pattern of calcined CTO:Yb,Er nanofibers.

scanning electron micrographs and transmission electron micrographs of the fibers produced in this study are shown in Figures 2a and 2b respectively. The inset image in Figure 2a shows that mean diameter of CTO nanofibers is approximately 80 nm. Lattice imaging revealed a d-spacing of 0.273 nm, which is attributable to the (200) planes of $CaTiO_3$ (JCPDS No.22-0153). Figure 2c shows well-defined X-ray diffraction peaks attributable to highly crystalline $CaTiO_3$ (JCPDS No.22-0153). The close match of the indexed reflections with the stick pattern suggests the absence of any extraneous Er or Yb compounds.

2.2 Synthesis of CTO-RB nanocomposite

To construct the CTO-RB composite, CTO nanofibers were first modified with amino groups to enhance the interaction between the two phases. FTIR spectra of CTO and amino-modified CTO nanofibers (CTO-NH_2) are shown in Figure 3a. For pure CTO nanofibers, a characteristic peak at 548 cm^{-1} can be ascribed to a Ti-O vibration. After modification using amino groups, a new peak appeared which can be assigned to N-H asymmetric bending vibration at 1560 cm^{-1}, indicating the successful functionalization of CTO nanofibers with amino groups.

To improve the reactivity of the carboxyl group for subsequent conjugation between RB and CTO nanofibers, the benzyl carboxyl group of RB was replaced with hexanoic acid (HA) to obtain RB-HA.[29] The FTIR spectrum of RB-HA in Figure 3a shows that a new peak corresponding to the C=O stretching vibration mode of the carboxyl group at 1720 cm^{-1}, confirming the successful preparation of RB-HA.

The nanofibers and photosensitizers were conjugated *via* electrostatic bonding between the amino group of CTO-NH_2 nanofibers and the carboxyl group of RB-HA. The C=O stretching vibration at 1720 cm^{-1} is absent in the FTIR spectrum of RBHA bound CTO nanofibers (CTO-RBHA, CTO-RB), whereas carboxylate bands at 1556 and 1390 cm^{-1} are detected, which indicates that proton transfer from the carboxylic acid of RB-HA to amino groups of the nanofibers has taken place.[30] The findings confirm that RB-HA adsorbed on the nanofibers *via* electrostatic interaction. The zeta potential of pure CTO nanofibers is -16 mV. Amino modification induced positive zeta potential of approximately + 21.7 mV for CTO-NH_2 nanofibers, and the introduction of RB-HA neutralized part of the positive charge on CTO-NH_2 nanofibers, resulting in a lower zeta potential of approximately + 6.5 mV (Figure 3b). The number of RB-HA molecules attached to CTO nanofibers was determined to be $1.77*10^{16}$ RB molecules per milligram of CTO nanofibers (Figure S1).

Under 980 nm excitation, the CTO nanofibers emit green light ($^2H_{11/2}$, $^4S_{3/2}$ → $^4I_{15/2}$ transition) and red light ($^4F_{9/2}$ → $^4I_{15/2}$ transition) (Figure 4a, blue trace) confirming successful doping of rare earth ions into $CaTiO_3$ crystal. The synergistic therapy platform is constructed based on the selective energy transfer from UCPL of CTO nanofibers to photosensitizers and AuNRs. RB was chosen in this study, because its absorption band at ~540 nm is overlapped by the green emission of CTO nanofibers when excited using radiation of 980 nm wavelength (Figure 4a). The absorption peaks of the CTO-RBHA complex around 500 – 600 nm present similar characteristics to the spectrum of pure RB-HA. The red shift observed may be attributed to the electron donating nature of the amine group.[31] Therefore, the emission of ~540 nm was strongly

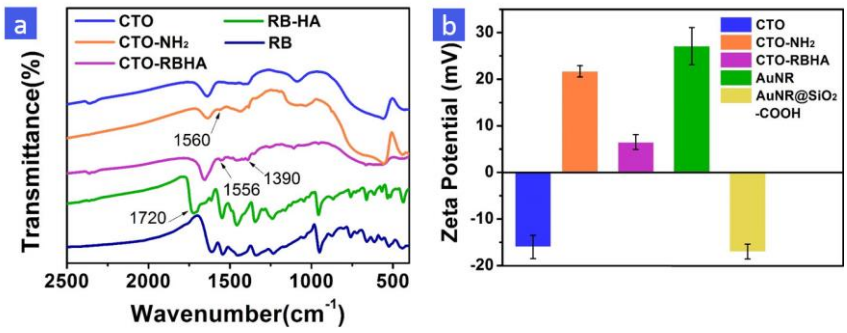

Figure 4 (a) FTIR spectra of RB molecules, RB-HA, CTO, CTO-NH_2 nanofibers and CTO-RBHA nanocomposite; (b) Zeta potentials of CTO, CTO-NH_2, CTO-RBHA, AuNRs and AuNR@SiO_2-COOH.

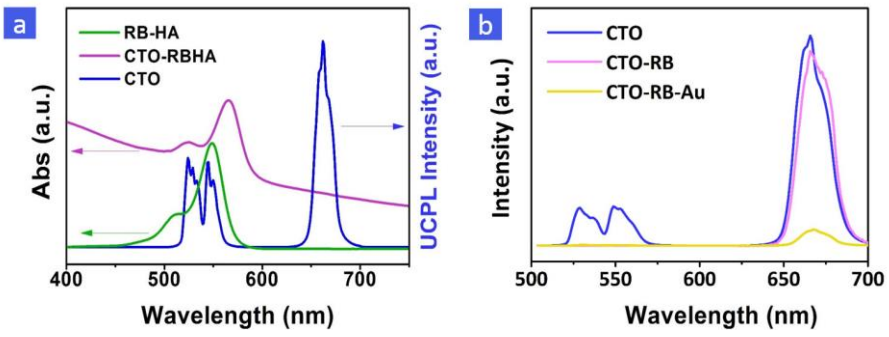

Figure 3 (a) UV-vis absorption spectra of RB-HA and CTO-RBHA, and upconversion emission spectrum of CTO nanofibers under 980 nm irradiation; (b) Up-conversion emission spectra of CTO, CTO-RB and CTO-RB-Au under 980 nm irradiation.

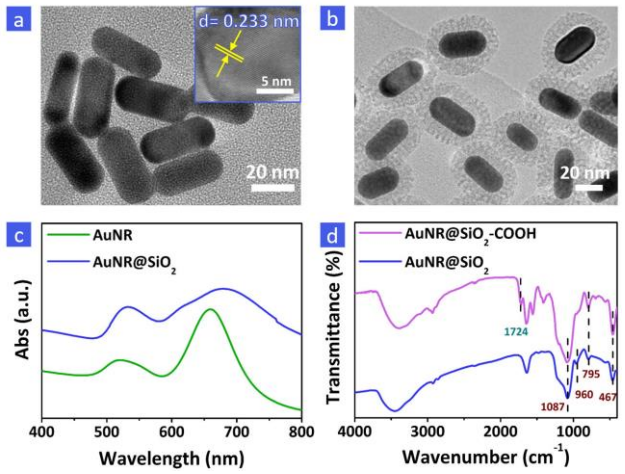

Figure 6 (a) TEM and HRTEM (inset) images of AuNRs; (b) TEM image of AuNRs@SiO_2, (c) UV-vis absorption spectra of AuNRs and AuNRs@SiO_2, (d) FTIR spectra of AuNR@SiO_2 and AuNR@SiO_2-COOH.

quenched while the emission of CTO nanofibers ~660 nm was almost unchanged after RB bonding, as demonstrated in Figure 4b, indicating the effective absorption of green emission by RB molecules.

2.3 Characteristics of CTO-RB-Au composite

AuNRs were prepared by a seed-mediated method with modifications.[32] The as-prepared AuNRs were coated with a bilayer of CTAB, which acts as a stabilizer. The CTAB-coated AuNRs had an average length of ~ 33.3 ± 7 and a width of ~ 14.4 ± 4 nm. The particles are crystalline with a d-spacing of 0.233 nm, corresponding to the (111) lattice plane of gold (JCPDS No. 04-0784) (Figure 5a). While gold is biologically inert and surface-bonded CTAB has low cytotoxicity, detached CTAB is a harmful surfactant.[33, 34] To reduce the potential hazards associated with this and also to improve photothermal stability, AuNRs were coated with silica.[35, 36] The CTAB layer acts as an organic template for the silica coating *via* a modified Stöber method. As shown in Figure 5b, the AuNRs obtained were coated with a SiO_2 layer with a thickness of approximately 10 nm. The corresponding UV-vis absorption spectra of AuNRs and AuNRs@SiO_2 further confirm the successful silica coating of AuNRs (Figure 5c). The AuNRs have a weak transverse surface plasmon resonance (TSPR) band at 520 nm and a strong longitudinal surface plasmon resonance (LSPR) band at 660 nm (as will be discussed below). After coating with SiO_2, a clear red shift of ~20 nm in the LSPR band compared with that of uncoated AuNRs was observed, which is attributed to the increase in the local refractive index of the surrounding medium after replacing CTAB with SiO_2 shell.[37, 38]

In order to anchor the AuNRs on the CTO-RB nanofibers, the AuNR@SiO_2 was modified with -COOH. The FTIR spectrum of AuNR@SiO_2 reveals asymmetric stretching of Si-O-Si at 1087 cm^{-1}, symmetric stretching of Si-O-Si at 795 cm^{-1}, a bending vibration for Si-O-Si at 467 cm^{-1} and symmetric stretching vibrations of Si-O bonds in the Si-OH groups at 960 cm^{-1}, which can be attributed to the SiO_2 layer (Figure 5d).[38, 39] After being modified with -COOH groups, a clear vibrational peak at 1724 cm^{-1} was observed, which can be assigned to the C=O stretching band of carboxylic groups. The zeta potential of AuNRs was found to be approximately + 27.1 mV. This was due to the bilayer of CTAB on the nanorod surface.[40] After silica coating and -COOH modification, the charge on the AuNRs reversed to -17 mV, indicating the successful synthesis of AuNR@SiO_2 –COOH (Figure 3b).

The AuNR@SiO_2-COOH obtained were conjugated to CTO-RB *via* electrostatic bonding (CTO-RB-Au). After assembly of AuNRs, it was observed that AuNRs assembled at the surface of nanofibers (Figure 6a). The UV-vis absorption of CTO-RB-Au combined the absorption spectra of CTO-RB and AuNR@SiO_2 (Figure 6b). Under 980 nm excitation, the CTO nanofibers emit green light ($^2H_{11/2}$, $^4S_{3/2}$ → $^4I_{15/2}$ transition) and red light ($^4F_{9/2}$ → $^4I_{15/2}$ transition). As discussed previously, the green emission of CTO nanofibers under 980 nm irradiation was absorbed by RB molecules because of the overlap between RB molecules and green emission of CTO nanofibers. Comparing the UCPL spectrum of CTO nanofibers and the LSPR absorption of AuNRs, an overlap was also observed in the red part of the spectrum (Figure 6b). Therefore, the red emission was subsequently absorbed after the CTO-RB nanofibers were conjugated with AuNRs (Figure 4b). It should be noted that the aspect ratio of Au nanoparticles presents the plasmon wavelength of the longitudinal resonance. Careful tuning of the ratio between the length and diameter of the AuNRs results in an aspect ratio of ~ 2. In this study, a longitudinal

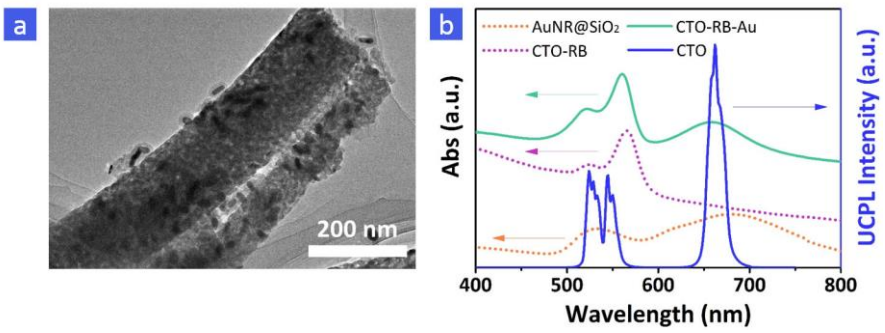

Figure 5 (a) TEM image of CTO-RB-Au nanocomposite; (b) UV-vis absorption spectra of CTO-RB, AuNR@SiO_2 and CTO-RB-Au, and up-conversion emission spectrum of CTO nanofibers under 980 nm irradiation.

plasmon resonance band at ~660 nm was achieved, which is vital prerequisite for spectral matching to the red regime of PL emission from CTO nanofibers. This unique design enabled maximized absorption of emission from CTO nanofibers under 980 nm irradiation and the consequent photothermal conversion.

Therefore, the consistent absorption of RB molecules and AuNRs in the CTO-RB-Au nanocomposite implied that a single wavelength laser, that is 980 nm, can be used to excite both PDT and PTT simultaneously.

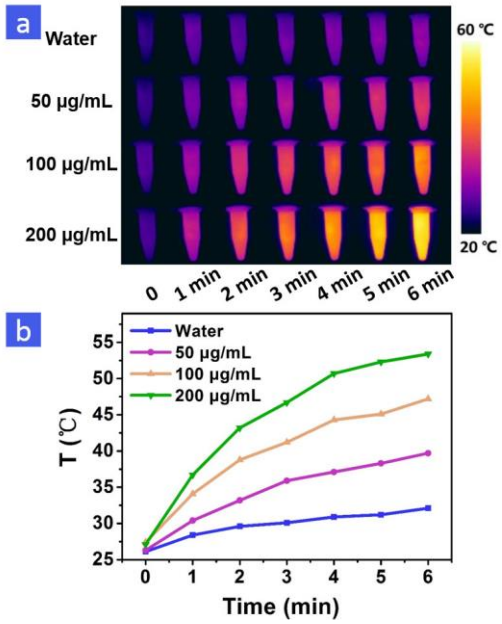

Figure 7 (a) Temperature images and (b) temperature variation of CTO-RB-Au nanocomposite solutions with different concentrations under irradiation by a 980-nm laser with a power density of 1.5W/cm^2 for 6 minutes.

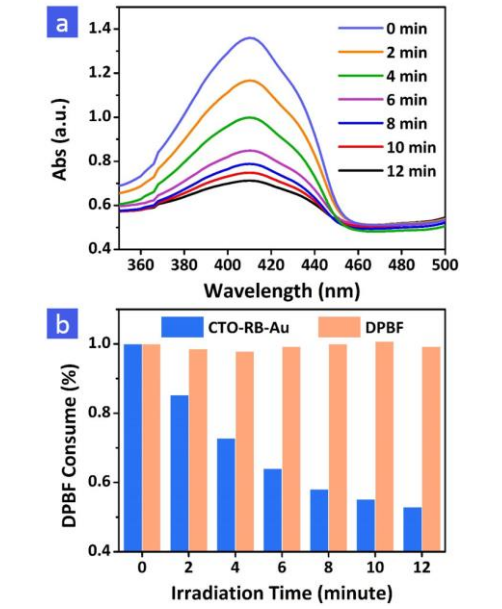

Figure 8 ROS generated from CTO-RB-Au nanocomposite. (a) UV-vis absorption spectra of a mixture of DPBF with CTO-RBHA-Au in ethanol under 980 nm irradiation (1.5W/cm^2) for 0-12 min respectively. (b) Consumption of DPBF over time in the presence and absence of CTO-RB-Au.

2.4 Photothermal and photodynamic effects

The temperature changes of aqueous solutions containing nanofibers of different concentrations under 980 nm laser irradiation (1.5 W/cm^2) was investigated to examine the photothermal effect of CTO-RB-Au nanofibers. Figure 7a presents real-time photographs of the aqueous solutions with different amounts of nanofibers captured by an infrared thermal camera. The temperature of deionized water without nanofibers only increased by 6 °C after irradiation for 6 min (Figure 7b). In contrast, the temperature of CTO-RB-Au solution rose rapidly and strongly depended on the concentration of nanofibers. The temperature of the solution with a concentration of 200 μg/mL, dramatically increased from 27.1 °C to 53.4 °C within 6 minutes. The findings confirm that the CTO-RB-Au nanocomposites can rapidly and efficiently convert the energy from 980 nm laser into thermal energy.

In addition to the photothermal effect, the ROS generation capability of CTO-RB-Au triggered by 980 nm light was also estimated using DPBF, a widely used chemical trapping reagent of $^1O_2$ that can irreversibly react with $^1O_2$.[41, 42] Under the irradiation of 980 nm light, the absorption of DPBF at 410 nm in pure DPBF solution remains unchanged (Figure 8). However, the absorbance of the solution containing CTO-RB-Au and DPBF decreased gradually with the increasing of irradiation time, indicating the decomposition of DPBF. After 12 min irradiation, ~ 50 % of DPBF was consumed, illustrating the efficient generation of singlet oxygen.

2.5 In vitro study

2.5.1 MTT assay

To evaluate the potential for biomedical application, the biocompatibility of CTO, CTO-RB, and CTO-RB-Au was firstly investigated. Hep G2 cells were incubated with different concentrations of the materials for 24 h and were then evaluated using an MTT assay to quantify cell viability. The results show that the cell survival can be maintained above 89 % from the lowest concentration of 12.5 μg/mL to the highest of 200 μg/mL, confirming the satisfactory biocompatibility of the three samples (Figure 9a). In addition, the cell viability under the 980-nm irradiation (1.5 W/cm^2) for 6 min was examined in the absence of the test materials (Figure 9a), to test the effect of the laser power alone. Survival of the Hep G2 cells remained at more than 90 %, implying that the toxicity presented by the laser power density was minimal. .

As designed, the CTO-RB-Au nanocomposite has potential for both PDT and PTT when irradiated at 980 nm. To assess the synergistic effect *in vitro*, the Hep G2 cell viability was quantified by changing the concentration of the nanocomposites and exposure time, respectively. As shown in Figure 9b, most of the cancer cells stayed alive when incubated with pure CTO nanofibers even under irradiation of NIR light. The fact that there was some limited levels of cell death in the highest concentration of 200 μg/mL can be attributed to the slight temperature rise caused by NIR light. When

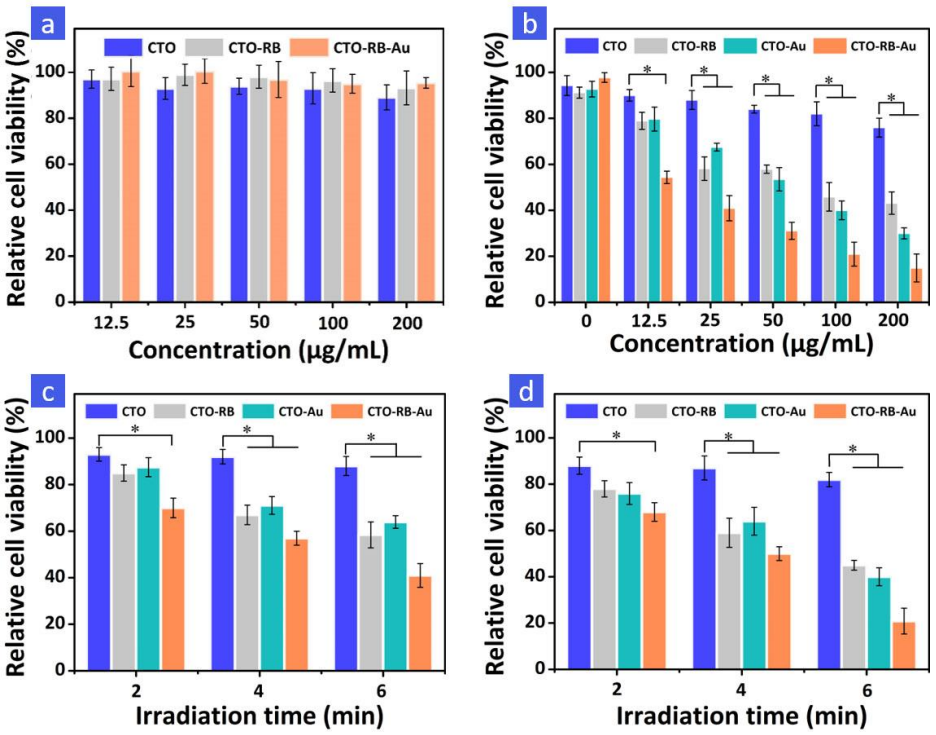

Figure 9 Relative cell viability of Hep G2 cells incubated with CTO, CTO-RB, and CTO-RB-Au. Cell viability at different concentrations (12.5-200 μg/mL) for 24 h (a) in the absence and (b) presence of 980 nm irradiation (1.5 W/cm^2) for 6 min. Cell viability depended on irradiation time (2-6 min) at concentration of (c) 25 μg/mL and (d) 100 μg/mL under 980 nm irradiation (1.5 W/cm^2), *$p < 0.05$.

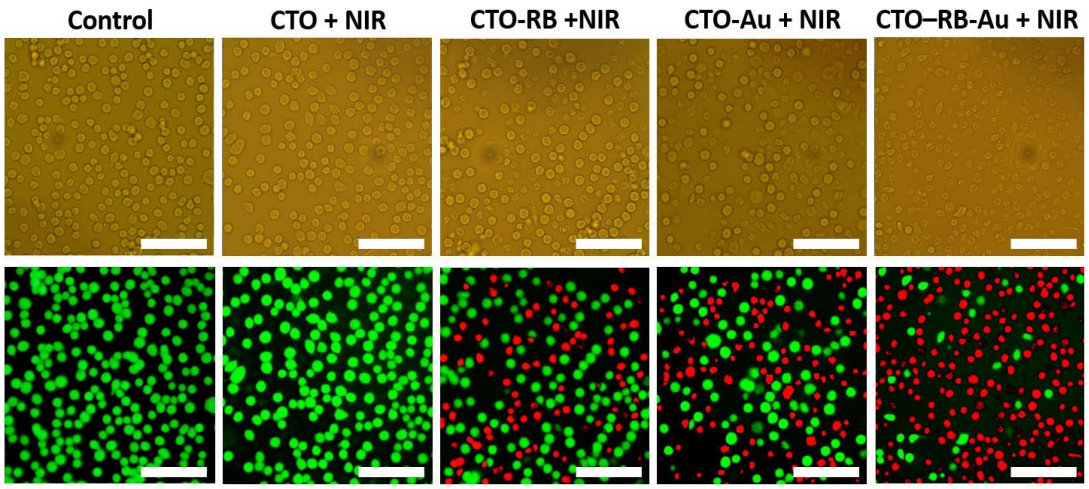

Figure 10 The bright field and fluorescence images of Calcein AM and PI co-staining Hep G2 cells cultured with CTO, CTO-RB, CTO-Au and CTO-RB-Au under 980 nm irradiation (1.5 W/cm^2, 6 min) with a nanofiber concentration of 100 μg/mL. Scale bars: 100 μm.

RB molecules were linked with CTO nanofibers there was a significant reduction in cell viability compared with pure CTO nanofibers and there was a dose-dependent photodynamic effect. A similar phenomenon was observed in the CTO-Au nanocomposite. About 60 % of Hep G2 cells were viable following single photodynamic or photothermal treatment with a concentration of 25 μg/mL and exposure to irradiation for 6 min. While when CTO-RB nanofibers were combined with AuNRs, the cell viability was dramatically decreased. Using a nanofiber concentration of 200 μg/mL, the cell viability declined to only 15 %, while for the CTO-RB sample, the figure was ~43 %. This shows that the *in vitro* anti-cancer efficacy of synergistic phototherapy is amplified 3 times as compared to the photodynamic approach alone. Moreover, as expected, the cell viability decreased with increasing irradiation time for the concentrations of 100 μg/mL and 25 μg/mL (Figure 9c&d). The results demonstrate that the CTO-RB-Au nanocomposite combining PDT and PTT has the potential to deliver cancer therapy with significantly improved efficiency.

2.5.2 Live/dead cell staining

The combined effects of PDT and PTT for CTO-RB-Au were further verified with Calcein AM and PI co-staining. Using 980 nm laser treatment, no obvious cell death was observed when cells were cultured with- the CTO nanofibers (Figure 10). However, in the CTO-RB and CTO-Au group, the number of live cells decreased as compared with the control group, indicating the cytotoxicity of ROS and the heat effect generated by CTO-RB and CTO-Au under excitation by the 980-nm laser, respectively. Furthermore, cell death was dramatically increased with CTO-RB-Au, as indicated by the sparse green fluorescence from live cells. The results agree with the MTT assay in Figure 9, clearly demonstrating again the efficient PDT/PTT effect of the CTO-RB-Au composite.

3 Conclusions

In summary, CTO-RB-Au nanocomposites have been successfully fabricated for use in an implantable device designed for use with combined photodynamic and photothermal therapy. In the composite, RB and AuNRs served as the PDT and PTT agents, respectively. Since RB and AuNRs have matched absorption with the green and red emissions of UCPL CTO nanofibers respectively, a laser with continuous single wavelength can be employed to induce the PDT and PTT effects simultaneously. Using 980 nm irradiation, the nanocomposite can convert energy effectively from NIR light to induce a combination of heat and ROS generation. Moreover, the results from *in vitro* experiments demonstrated that this simultaneous therapeutic approach was significantly more effective than PDT alone. The synergistic combination of PDT and PTT thus holds promise for future applications in multiple anticancer therapies.

4 Experimental section

4.1 Synthesis of CTO nanofibers

A method for the preparation and electospinning of CTO nanofibers has been reported previously.[27, 28] Briefly, a typical sol-gel approach was used to prepare the precursor solution for electrospinning. Tetrabutyl titanate (~0.82 g), $Ca(NO_3)_2{\cdot}4H_2O$ (~0.45 g), $Yb(NO_3)_3{\cdot}5H_2O$ (~0.19 g) and $Er(NO_3)_3{\cdot}5H_2O$ (~0.02 g) were mixed with acetic acid (2 mL), ethanol (7 mL) and N, N-dimethylformamide (DMF, 3 mL) by stirring for 3 h. Then 0.6 g of poly(vinylpyrrolidone) (PVP , MW = 1,300,000, Aladdin), 0.2 g of Pluronic® F127 ($EO_{106}PO_{70}EO_{106}$) and 0.5 mL of acetyl acetone were added and stirred overnight to obtain a homogeneous solution.

During the electrospinning process, the precursor was fed into a stainless-steel needle at 0.4 mL/h. When a voltage of 6-8 kV was applied to the needle, a stable cone-jet electrospinning mode was achieved and this was monitored using a high-speed camera (Baumer, TXG04h, Germany). Uniform precursor nanofibers were formed and collected on aluminum foil. After the product had been vacuum-dried at 80 °C for 12 h to remove the residual solvent, the nanofibers were calcined at 700 °C for 2 h in air.

4.2 Surface decoration of CTO nanofibers

CTO nanofibers were firstly modified with amino groups using a protocol adapted from work by Maldiney et al.[43] and our previous work[27, 28], in which 100 mg of CTO nanofibers were dispersed in NaOH aqueous solution (80 mL, 5 mM) under stirring for 12 h. Then the nanofibers were collected, washed, and dried. Thereafter, the obtained nanofibers were mixed with 500 µL of (3-aminopropyl) triethoxysilane (APTES, Aladdin) in 40 mL of DMF by stirring at 80 °C for 24 h. Then the amino modified CTO nanofibers were washed with DMF and collected by centrifugation.

4.3 Linking of RB with CTO nanofibers

To improve the reactivity of the carboxyl group for RB, RB hexanoic acid ester (RB-HA) was firstly synthesized using a method described by Lamberts et al..[29] Briefly, 100 mg of RB was reacted with 20 mg of 6-bromohexanoic acid in 25 mL DMF at 70 °C for 24 h to obtain RB-HA aqueous solution. Subsequently, tris-(2-hydroxyethyl)-amine (TEA, 80 µL), N-hydroxysuccinimide (NHS, 60 mg) and N-(3-dimethylaminopropyl)-N'-ethylcarbodiimide hydrochloride (EDC, 120 mg) were added into the RB-HA solution and stirred at 30 °C for 1 h. Our novel step was to then introduce 60 mg of CTO-NH_2 nanofibers into the solution. The mixture was stirred for 24 h to obtain RB-HA conjugated CTO nanofibers. All experiments were undertaken in black-out conditions.

4.4 Synthesis of gold nanorods

4.4.1 Seed solution

The gold nanorods (AuNRs) were fabricated according to the well-established seed-mediated growth method with some modifications.[32] Briefly, CTAB aqueous solution (5 mL, 0.2 M) was mixed with $HAuCl_4$ (5 mL, 0.5 mM) and ice-cold $NaBH_4$ (0.6 mL, 0.01M) under vigorous stirring for 2 min. Then the brownish-yellow seed solution was aged at room temperature for 30 min before use.

4.4.2 Growth solution

The growth solution was made from solutions of CTAB (50 mL, 0.1 M), sodium salicylate (0.16 g), $HAuCl_4$ (50 mL, 1 mM), $AgNO_3$ (1.2 mL, 4 mM) and ascorbic acid (0.2 mL, 0.064 M). The growth solution became colorless after gentle stirring. The gold seed solution (0.16 mL) was then injected into the growth solution and the mixture was stirred for 30 s and left undisturbed at 30 °C overnight. The gold nanorods obtained were centrifuged, washed with deionized water to removed excess CTAB and dispersed in 10 mL of water for further use.

4.5 Synthesis of carboxyl-modified silica-coated gold nanorods

Carboxyl-modified silica-coated gold nanorods (AuNR@SiO_2-COOH) were prepared based on a modified version of a method reported previously.[44, 45] The as-synthesized AuNRs in 10 mL of water was mixed with NaOH aqueous solution (0.1 mL, 0.1 M) under stirring. Then 100 µL of 5 % TEOS in methanol were added three times at 30 min intervals, and the mixture was reacted for 12 h. The obtained AuNR@SiO_2 were centrifuged, washed with deionized water several times, and re-dispersed in 5 mL of ethanol for further use.

The AuNR@SiO_2 solution and 40 µL of APTES were mixed in 40 mL of DMF and stirred for 24 h. Then the obtained amino modified

AuNR@SiO_2 (AuNR@SiO_2-NH_2) were centrifuged and redispersed in 5 mL of ethanol.

The AuNR@SiO_2-NH_2 solution, 40 mg of succinic anhydride (SA) and 40 mg of triethylamine were added into 5 mL DMSO and stirred in 40 °C for 48 h to obtain AuNR@SiO_2-COOH. 20 mg of AuNR@SiO_2-COOH and 40 mg of the CTO nanofibers were combined by stirring for 24 h to obtain a AuNR conjugated CTO nanocomposite (CTO-Au). Similarly, 20 mg of AuNR@SiO_2-COOH and 40 mg of the CTO-RB composite were combined by stirring for 24 h to obtain RB and AuNRs co-conjugated CTO nanocomposite.

4.6 Examination of photothermal performance

The photothermal effect of CTO-RB-Au solutions with different concentrations (0, 50, 100, 200 μg/mL) were estimated using a 980 nm laser at a power density of 1.5 W/cm^2 for up to 6 min at room temperature using a fiber coupled laser source (Stone laser system AC90-260V/50-60HZ, China). An infrared thermal imaging instrument (FLIR, E40) was used to measure and map the change of temperature.

4.7 Detection of singlet oxygen generation

Singlet oxygen generation irradiated by 980 nm light was measured by the absorption of a chemical probe, 3-diphenylisobenzofuran (DPBF). 2 mL of CTO-RB-Au ethanol solution (5 mg/mL) were mixed with 1 mL of DPBF ethanol solution (50 mM). Absorbance of the solution at 410 nm was recorded every 1 min. The generation of $^1O_2$ was determined from the decline of the absorption of DPBF. Absorption of DPBF solution under irradiation in the absence of materials was also recorded as a negative control.

4.8 Preliminary *in vitro* study

Human Hep G2 liver cancer cells were used to examine the *in vitro* antitumor potentials of CTO-RB-Au platform. The cytotoxicity of CTO, CTO-RB, CTO-Au and CTO-RB-Au was determined using a 3-(4,5-dimethylthiazol-2-yl)-2,5-diphenyltetrazolium bromide (MTT) cell assay. Hep G2 cells were seeded in a 96-well plate at a density of 8000 cells per well and incubated at 37 °C for 24 h. Then the culture media was replaced with fresh culture medium containing CTO, CTO-RB, CTO-Au and CTO-RB-Au nanocomposites at different concentrations. To study the photodynamic and photothermal effect, the nanocomposites were irradiated using a 980-nm laser for 0-6 minutes with an energy density of 1.5W/cm^2. After incubation for 24 h, 10 μL of MTT solution was added into each well and cultured for 4 h. Then the original medium was removed and formazan (MTT metabolic product) was dissolved with dimethyl sulfoxide (DMSO, 100 μL per well). The absorbance of the solution was measured at 490 nm using a microplate reader (Tecan 50, The Switzerland). The anticancer effect was further visualized using calcein acetoxymethyl ester (calcein AM) and propidium iodide (PI) staining and observed with a fluorescent microscope (Nexcope, The USA). The samples (not irradiated and/or not treated with nanocomposite) were used as a test control. Similarly, the cytocompatibility of samples was examined using an MTT assay with Hep G2 cells, following the same procedure above.

4.9 Characterization

The microstructure and morphology of materials were visualized by a Hitachi SU-70 field-emission scanning electron microscope (FESEM) and a FEI Tecnai F20 high-resolution transmission electron microscope (HRTEM). A thermo ARL X'TRA powder diffractometer was used to record the X-ray diffraction (XRD) patterns. FTIR spectra were evaluated using a Perkin-Elmer 580B infrared spectrophotometer (Tensor 27, Bruker). A Zetasizer (Zetasizer 3000 HSA, Malvern) was used to determine the zeta potential of samples at room temperature. The UV-vis-NIR absorption spectra were examined by TU-1810 UV-vis spectrophotometer. The UCPL spectra were recorded using a fluorescence spectrophotometer (PL, FLSP920, Edinburgh) under the excitation of a 980 nm laser. The fiber diameter and the size of gold nanorods were measured from SEM or TEM micrographs using image analysis (n = 50).

4.10 Statistical Analysis

Data were expressed as mean ± standard deviation (SD). All statistical data were obtained using a two-tailed Student's t test. A value of $p < 0.05$ was taken as statistically significant.

Acknowledgements

This work was financially supported by the National Nature Science Foundation of China (51232006 and 51672247), the '111' Program funded by Education Ministry of China and State Administration of Foreign Experts Affairs (B16043), the Major State Research Program of China (2016YFC1101900), and the Nature Science Foundation of Zhejiang Province (LY15E020005).

Notes and references

1. L. A. Torre, F. Bray, R. L. Siegel, J. Ferlay, J. Lortet-Tieulent and A. Jemal, *CA-Cancer J. Clin.*, 2015, **65**, 87-108.
2. X.-B. Xiong and A. Lavasanifar, *ACS Nano*, 2011, **5**, 5202-5213.
3. D. B. Longley and P. G. Johnston, *J. Pathol.*, 2005, **205**, 275-292.
4. C. S. Gutsche, M. Ortwerth, S. Gräfe, K. J. Flanagan, M. O. Senge, H.-U. Reissig, N. Kulak and A. Wiehe, *Chem-Eur J*, 2016, **22**, 13953-13964.
5. G. Chang, Y. Wang, B. Gong, Y. Xiao, Y. Chen, S. Wang, S. Li, F. Huang, Y. Shen and A. Xie, *ACS Appl. Mater. Interfaces*, 2015, **7**, 11246-11256.
6. Q. Chen, C. Wang, L. Cheng, W. He, Z. Cheng and Z. Liu, *Biomaterials*, 2014, **35**, 2915-2923.
7. C. Qin, J. Fei, A. Wang, Y. Yang and J. Li, *Nanoscale*, 2015, **7**, 20197-20210.
8. M. Yu, F. Guo, J. Wang, F. Tan and N. Li, *ACS Appl. Mater. Interfaces*, 2015, **7**, 17592-17597.
9. M. G. Walker, P. J. Jarman, M. R. Gill, X. Tian, H. Ahmad, P. A. N. Reddy, L. McKenzie, J. A. Weinstein, A. J. H. M. Meijer, G. Battaglia, C. G. W. Smythe and J. A. Thomas, *Chem-Eur J*, 2016, **22**, 5996-6000.
10. R. Weissleder, *Nat Biotech*, 2001, **19**, 316-317.
11. D. Zhang, M. Wu, Y. Zeng, L. Wu, Q. Wang, X. Han, X. Liu and J. Liu, *ACS Appl. Mater. Interfaces*, 2015, **7**, 8176-8187.

12. B. Wang, J.-H. Wang, Q. Liu, H. Huang, M. Chen, K. Li, C. Li, X.-F. Yu and P. K. Chu, *Biomaterials*, 2014, **35**, 1954-1966.
13. L. Liang, Y. Lu, R. Zhang, A. Care, T. A. Ortega, S. M. Deyev, Y. Qian and A. V. Zvyagin, *Acta Biomater.*, 2017, **51**, 461-470.
14. Q. Sun, Q. You, X. Pang, X. Tan, J. Wang, L. Liu, F. Guo, F. Tan and N. Li, *Biomaterials*, 2017, **122**, 188-200.
15. B. Du, X. Gu, W. Zhao, Z. Liu, D. Li, E. Wang and J. Wang, *J. Mater. Chem. B*, 2016, **4**, 5842-5849.
16. M. Nurunnabi, Z. Khatun, G. R. Reeck, D. Y. Lee and Y.-k. Lee, *ACS Appl. Mater. Interfaces*, 2014, **6**, 12413-12421.
17. H. Gong, L. Cheng, J. Xiang, H. Xu, L. Feng, X. Shi and Z. Liu, *Adv. Funct. Mater.*, 2013, **23**, 6059-6067.
18. X. Sun, B. Dong, H. Xu, S. Xu, X. Zhang, Y. Lin, L. Xu, X. Bai, S. Zhang and H. Song, *ACS Appl. Mater. Interfaces*, 2017, **9**, 11451-11460.
19. L. Yan, Z. Wang, X. Chen, X.-J. Gou, Z. Zhang, X. Zhu, M. Lan, W. Chen, G. Zhu and W. Zhang, *Chem. Commun.*, 2017, **53**, 2339-2342.
20. A. E. O'Connor, W. M. Gallagher and A. T. Byrne, *Photochem. Photobiol.*, 2009, **85**, 1053-1074.
21. X. Tan, J. Wang, X. Pang, L. Liu, Q. Sun, Q. You, F. Tan and N. Li, *ACS Appl. Mater. Interfaces*, 2016, **8**, 34991-35003.
22. R. De Souza, P. Zahedi, C. J. Allen and M. Piquette-Miller, *Drug Delivery*, 2010, **17**, 365-375.
23. J. B. Wolinsky, Y. L. Colson and M. W. Grinstaff, *J. Controlled Release*, 2012, **159**, 14-26.
24. P. Huang, K. W. Xu and Y. Han, *Mater. Lett.*, 2005, **59**, 185-189.
25. H. Tang and F. Wang, *Mater. Lett.*, 2013, **93**, 427-430.
26. J. P. Wiff, V. M. Fuenzalida, J. L. Arias and M. S. Fernandez, *Mater. Lett.*, 2007, **61**, 2739-2743.
27. H. Liu, Y. Fu, Y. Li, Z. Ren, X. Li, G. Han and C. Mao, *Langmuir*, 2016, **32**, 9083-9090.
28. X. Li, Q. Zhang, Z. Ahmad, J. Huang, Z. Ren, W. Weng, G. Han and C. Mao, *J. Mater. Chem. B*, 2015, **3**, 7449-7456.
29. J. J. M. Lamberts, D. R. Schumacher and D. C. Neckers, *J. Am. Chem. Soc.*, 1984, **106**, 5879-5883.
30. B. Muñoz, A. Rámila, J. Pérez-Pariente, I. Díaz and M. Vallet-Regí, *Chem. Mater.*, 2003, **15**, 500-503.
31. S. W. Prasanna, G. Poorani, M. S. Kumar, P. Aruna and S. Ganesan, *Mater. Express*, 2014, **4**, 359-366.
32. X. Ye, L. Jin, H. Caglayan, J. Chen, G. Xing, C. Zheng, V. Doan-Nguyen, Y. Kang, N. Engheta, C. R. Kagan and C. B. Murray, *ACS Nano*, 2012, **6**, 2804-2817.
33. X. Hu and X. Gao, *Phys. Chem. Chem. Phys.*, 2011, **13**, 10028-10035.
34. C.-W. Chen, P.-H. Lee, Y.-C. Chan, M. Hsiao, C.-H. Chen, P. C. Wu, P. R. Wu, D. P. Tsai, D. Tu, X. Chen and R.-S. Liu, *J. Mater. Chem. B*, 2015, **3**, 8293-8302.
35. L. C. Chen, C. W. Wei, J. S. Souris, S. H. Cheng, C. T. Chen, C. S. Yang, P. C. Li and L. W. Lo, *J. Biomed. Opt.*, 2010, **15**, 6.
36. Y. S. Chen, W. Frey, S. Kim, K. Homan, P. Kruizinga, K. Sokolov and S. Emelianov, *Opt. Express*, 2010, **18**, 8867-8877.
37. Z. Zhang, L. Wang, J. Wang, X. Jiang, X. Li, Z. Hu, Y. Ji, X. Wu and C. Chen, *Adv. Mater.*, 2012, **24**, 1418-1423.
38. D.-W. Wang, X.-M. Zhu, S.-F. Lee, H.-M. Chan, H.-W. Li, S. K. Kong, J. C. Yu, C. H. K. Cheng, Y.-X. J. Wang and K. C.-F. Leung, *J. Mater. Chem. B*, 2013, **1**, 2934-2942.
39. F. Liu, J. Wang, P. Huang, Q. Zhang, J. Deng, Q. Cao, J. Jia, J. Cheng, Y. Fang, D. Y. B. Deng and W. Zhou, *J. Mater. Chem. B*, 2015, **3**, 2206-2214.
40. B.-K. Wang, X.-F. Yu, J.-H. Wang, Z.-B. Li, P.-H. Li, H. Wang, L. Song, P. K. Chu and C. Li, *Biomaterials*, 2016, **78**, 27-39.
41. D. Yang, G. Yang, S. Gai, F. He, R. Lv, Y. Dai and P. Yang, *ACS Biomater.-Sci. Eng.*, 2016, **2**, 2058-2071.
42. X.-S. Ke, Y. Ning, J. Tang, J.-Y. Hu, H.-Y. Yin, G.-X. Wang, Z.-S. Yang, J. Jie, K. Liu, Z.-S. Meng, Z. Zhang, H. Su, C. Shu and J.-L. Zhang, *Chem-Eur J*, 2016, **22**, 9676-9686.
43. T. Maldiney, A. Bessiere, J. Seguin, E. Teston, S. K. Sharma, B. Viana, A. J. J. Bos, P. Dorenbos, M. Bessodes, D. Gourier, D. Scherman and C. Richard, *Nat. Mater.*, 2014, **13**, 418-426.
44. Q. Jia, J. Ge, W. Liu, S. Liu, G. Niu, L. Guo, H. Zhang and P. Wang, *Nanoscale*, 2016, **8**, 13067-13077.
45. W.-C. Wu and J. B. Tracy, *Chem. Mater.*, 2015, **27**, 2888-2894.